AD-A069 091 MASSACHUSETTS INST OF TECH LEXINGTON LINCOLN LAB F/G 20/5
ELECTROOPTICAL DEVICES.(U)
SEP 78 C E HURWITZ F19628-78-C-0002

UNCLASSIFIED ESD-TR-78-394 NL

END
DATE FILMED
7-79
DDC

(12)

MASSACHUSETTS INSTITUTE OF TECHNOLOGY

LINCOLN LABORATORY

ELECTROOPTICAL DEVICES

SEMIANNUAL TECHNICAL SUMMARY REPORT TO THE ROME AIR DEVELOPMENT CENTER

1 APRIL – 30 SEPTEMBER 1978

ISSUED 30 MARCH 1979

LEXINGTON MASSACHUSETTS

ABSTRACT

This report covers work carried out with support of the Department of the Air Force during the period 1 April through 30 September 1978. A part of this support was provided by the Rome Air Development Center.

The current objectives of the electrooptical device program are: (1) to perform life tests on GaInAsP/InP double-heterostructure (DH) diode lasers operating in the 1.0- to 1.3-μm-wavelength region and analyze the degradation mechanisms, and (2) to fabricate and study avalanche photodiodes of similar composition GaInAsP operating in the same wavelength region.

Threshold current densities in DH GaInAsP/InP stripe geometry lasers have been reduced to 2 to 3 kA/cm^2, which, together with new mounting procedures designed to reduce thermal resistance, have resulted in improved performance at elevated temperatures. Considerably lengthened lifetimes and meaningful accelerated aging studies at temperatures as high as 70°C should now be possible.

Values of gain as high as 18 with concurrent dark currents of 20 μA have been achieved in GaInAsP/InP inverted mesa photodiodes. Rise and fall times of less than 60 psec in detector pulse response have been measured.

Multi-energy Be implants in n-type InP and GaInAsP have yielded layers with uniform as-implanted Be concentrations of approximately $3 \times 10^{18}\ cm^{-3}$. Sheet carrier concentrations of 1 to $2 \times 10^{14}\ cm^{-2}$ were obtained on samples implanted at room temperature and annealed at 750° and 700°C for InP and GaInAsP, respectively.

Improved p-n junction diodes have been formed by Be-implantation in n-type InP and GaInAsP. Subnanoampere leakage currents and abrupt voltage breakdowns were observed for both mesa and planar InP diodes. Scanning photoresponse measurements of the GaInAsP ($E_g \approx 1.0$ eV) mesa diodes showed uniform avalanche gains of 2 to 3 times.

Liquid-phase epitaxy is now being used to reproducibly grow InP and GaInAsP alloys with $N_D - N_A$ at the low $10^{15}\ cm^{-3}$ level. The 77 K electron mobilities for the InP are in the 40,000 to 60,000 cm^2/V-sec range, with N_D/N_A between 2.5 and 6. For $Ga_{0.2}In_{0.8}As_{0.5}P_{0.5}$, the 77 K mobilities are 12,000 to 14,000 cm^2/V-sec with $N_D/N_A \leq 2$.

Analysis of measurements of the high-magnetic-field Hall coefficient vs temperature yields values for the concentrations of deep donors in InP and GaInAsP specimens of $5 \times 10^{15}\ cm^{-3}$ and $3 \times 10^{14}\ cm^{-3}$, respectively. The transport data were fit using deep-level donor activation energies of 0.29 and 0.12 eV for InP and GaInAsP, respectively. These energy values were inferred from the photoluminescence spectra.

In a study of photoluminescence of LPE-grown InP and GaInAsP, several spectral peaks were observed in a range 0.3 to 1.41 eV. It is hypothesized that one of the peaks in the photoluminescence spectra, with peak energies of 1.12 eV for InP and 0.9 eV for GaInAsP, is due to oxygen.

The oscillatory interband magnetotransmission has been measured on samples of LPE-grown $Ga_{0.23}In_{0.77}As_{0.52}P_{0.48}$ layers. The band parameters determined from the analysis of the data are $E_g = 1.07$ eV, $m_c^* = 0.061\ m_o$, and $E_p = 17.6$ eV, where these parameters are the direct energy gap at $T \approx 20$ K, the conduction-band effective mass, and the $\vec{k} \cdot \vec{p}$ interaction energy, respectively.

CONTENTS

ELECTROOPTICAL DEVICES

I. GaInAsP/InP DH LASERS

A. OVERVIEW

Following the previously discussed[1] elimination of the rapid short-term deterioration of GaInAsP/InP lasers by appropriate cleaning procedures, the dominant degradation mode of the current lasers appears to be an increase during CW operation of the thermal resistance between the active region of the device and the heat sink. Recent reductions in the threshold current densities of LPE-grown wafers have significantly reduced this problem. Previously, the threshold current densities in stripe-geometry lasers with 13-μm-wide stripes defined by proton bombardment have been in the 4- to 6-kA/cm^2 range. Recent wafers have yielded devices with threshold current densities in the range of 2 to 3 kA/cm^2 and in which the power dissipation is therefore reduced by factors of 2 to 3, depending on the series electrical resistance. Our initial results with a low-threshold device show no measurable increase in pulsed or CW threshold current and no change in efficiency after 3500 hr of CW operation at 22°C.

Nevertheless, at the higher temperatures required for accelerated aging studies (up to ≃70°C), the thermal resistance again becomes unstable and increases with time in response to the increase in the threshold current (and consequently the power dissipation) with increasing temperature. A new mounting procedure has therefore been developed which appears to improve the stability of the thermal resistance at elevated temperatures. One device so fabricated has been operating CW at 50°C for over 800 hr without measurable degradation. The results indicate that considerably lengthened room-temperature lifetimes are now possible, and that meaningful accelerated aging studies at 70°C can now be undertaken.

In the following sections, lasers fabricated from one of these new low-threshold wafers will be characterized and more-extensive life-test data will be presented.

B. PERFORMANCE CHARACTERISTICS OF WAFER 4-4-78

The relatively low-threshold devices made from wafer 4-4-78 not only exhibit low rates of degradation, as discussed in the next sections, but also show improved characteristics important for applications involving transmission through optical fibers.

Figure I-1 shows the CW light output from one laser facet vs current at several heat-sink temperatures for a device operating at a (room-temperature) wavelength of 1.285 μm. The differential external quantum efficiency is about 40 percent from one facet. The light output is not perfectly linear with current, and a noticeable "kink" occurs in most devices at 5 to 8 mW of output power. However, nearly linear behavior is obtained for outputs of more than 4 mW.

As seen in Fig. I-2(a), multimode operation is observed near threshold; but for currents 10 to 15 percent above threshold, the lasers typically operate with nearly all the power in a single longitudinal mode as seen in Fig. I-2(b). The scans of the mirror-illumination pattern and the far-field pattern shown in Fig. I-3(a-b) indicate that the lateral-mode pattern (parallel to the junction) appears to be of the lowest spatial order, even at currents well above the nonlinear "kink" region of the light output characteristic. The full width of the beam in the far field at half-maximum is about 7°, which for a Gaussian beam would correspond to a full width

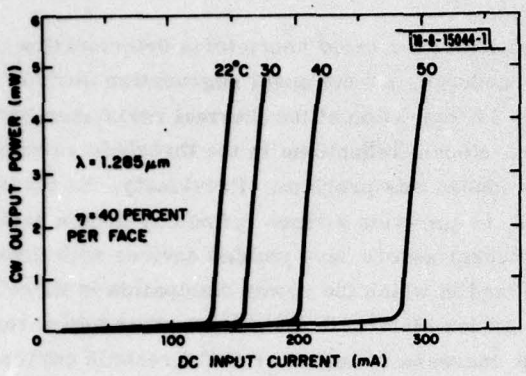

Fig. I-1. Light output vs current of a GaInAsP/InP DH laser at heat-sink temperatures of 22° to 50°C. Differential external quantum efficiency is as high as 40 percent per face.

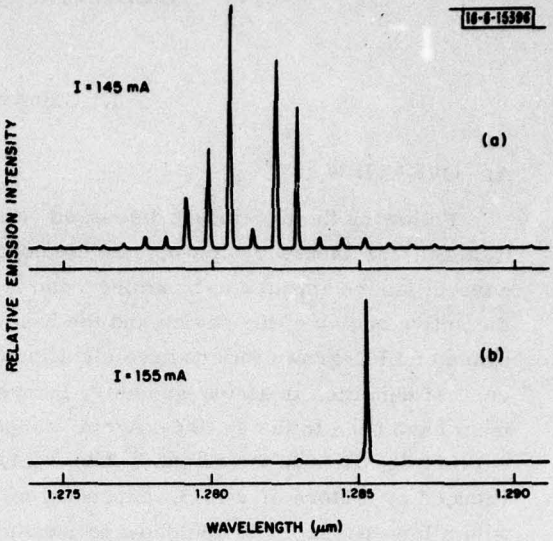

Fig. I-2. Spectra at room temperature for DH laser of Fig. I-1 at two current levels: (a) 5 percent above threshold, and (b) 12 percent above threshold.

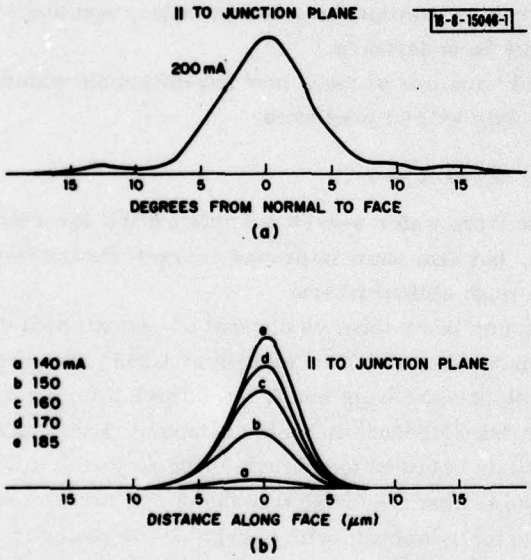

Fig. I-3. (a) Far-field pattern, and (b) mirror-illumination pattern of a DH laser in plane parallel to junction.

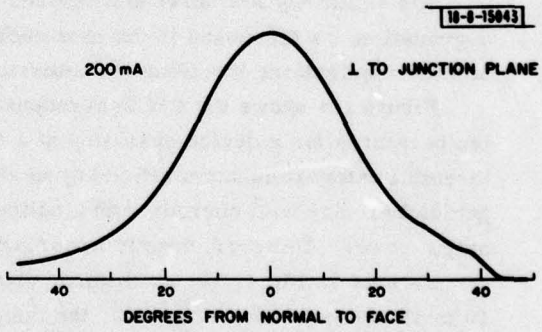

Fig. I-4. Far-field pattern of a DH laser measured in plane perpendicular to junction.

at half-maximum of 4.6 μm at the mirror. This value (within the resolution of the measurement, which is about 1.5 μm) agrees with that obtained from the mirror-illumination scans shown in Fig. I-3. The mode pattern in the transverse direction (perpendicular to the junction plane) also appears to be of the lowest spatial order, as seen in the far-field pattern of Fig. I-4. The full beamwidth at half-maximum is about 36°, corresponding to a full width at half-maximum of 0.85 μm at the mirror. This value is beyond the resolution capability of the mirror-illumination measurement, but is not unreasonable.

C. ROOM-TEMPERATURE LIFE TESTS

One of the devices from wafer 4-4-78 has been operating at room temperature (22°C) with a CW output from one facet of more than 4 mW for 3500 hr. The threshold current density of this device is 2.9 kA/cm^2. In Fig. I-5, the pulsed and CW threshold currents vs CW operating time for this device are compared with the data for a device from another wafer (1-28-77) which had a much higher CW threshold current density (7.4 kA/cm^2) and which operated for 7800 hr before failure. Because of the power dissipation in the latter device, a substantial difference is seen between the CW and pulsed thresholds, a difference which is not seen in the device from wafer 4-4-78. Although a small increase in pulsed threshold was observed near the end of life (a rise of less than 2 percent per thousand hours), the end of life is clearly due to the rapid rise of the CW threshold as the thermal resistance begins to increase after a few thousand hours of operation. The pulsed and CW thresholds of the device from wafer 4-4-78 were last measured at 2000 hr of operation where they both were still unchanged from their initial values. Since that time, the device has continued to run with no change in output power, from which we may infer no change in CW threshold or in efficiency, up to the present 3500 hr of operation.

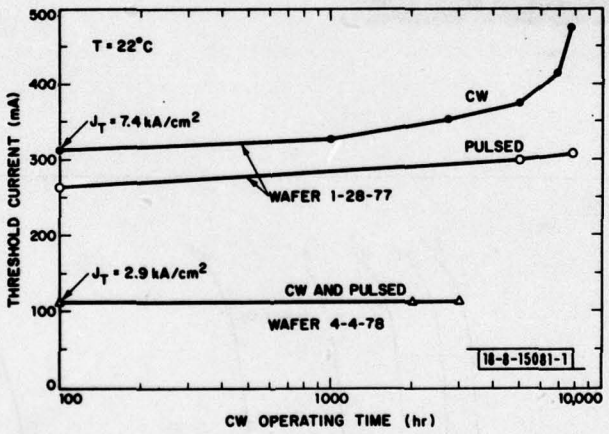

Fig. I-5. Comparison of pulsed and CW threshold currents as a function of CW operating time for a device from a relatively high-threshold wafer (1-28-77) and a device from a relatively low-threshold wafer (4-4-78).

D. ACCELERATED AGING AT ELEVATED TEMPERATURES

If the device, whose light output vs current is shown in Fig. I-1, were to be operated at 50°C at an output power of 4 mW, the operating current required would be 300 mA rather than the 140 mA required at 22°C, and the current density would be of the order of 6 kA/cm^2. When

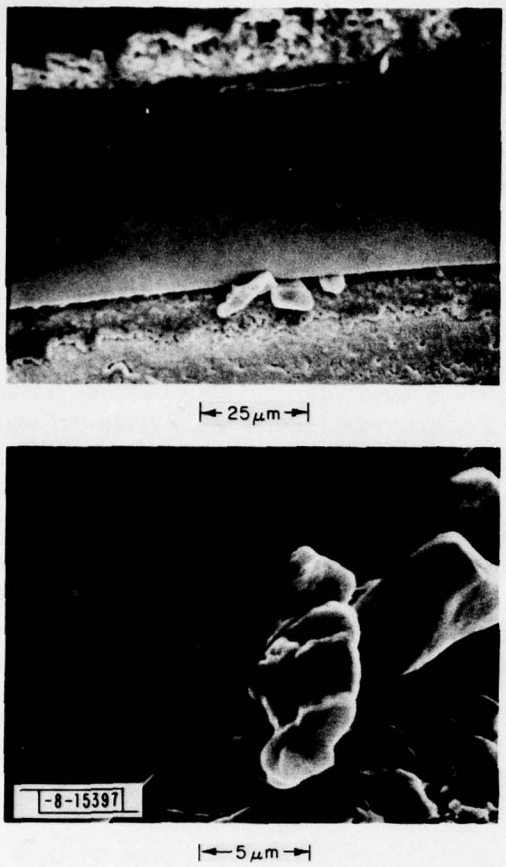

Fig. I-6. Scanning electron micrographs of output face of a DH laser which failed during operation at 50°C, apparently from a short circuit caused by indium extended from beneath device. As seen in lower view, indium makes contact with face.

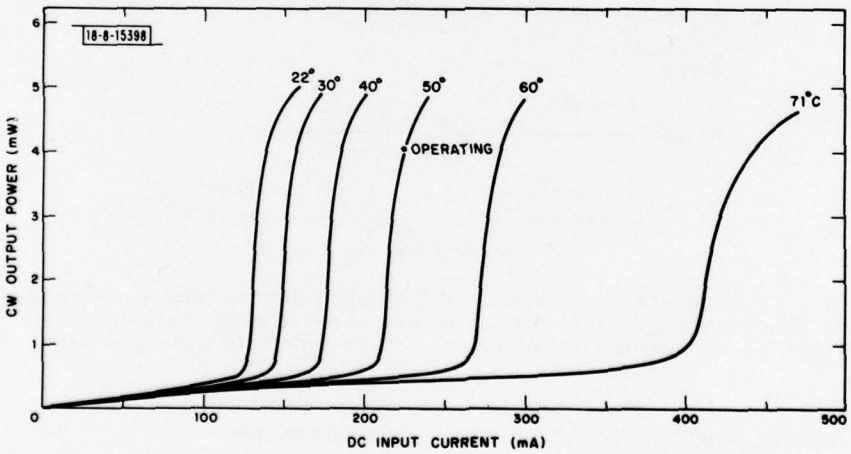

Fig. I-7. Light output vs current of a DH laser from wafer 4-4-78 at heat-sink temperatures between 22° and 71°C.

such a device was actually tested under such conditions, it showed a gradual decline in output power for about 50 hr, then a more rapid decline followed by an abrupt drop to no output at 72 hr of operation. The immediate cause of failure in this case appeared to be extrusion of the indium solder from beneath the device up onto the facet, thus causing an electrical short circuit of the device (see Fig. I-6). The gradual degradation prior to that time, however, was most likely due to the familiar increase of thermal resistance. In any event, physical movement of the indium solder was clearly evident.

In order to eliminate this problem, we have developed techniques to minimize the amount of indium under the devices. The copper heat sinks on which the laser chips were mounted were carefully machined flat to within 0.25 μm, and the thickness of the indium used to solder the device was decreased to about 5 μm. Devices mounted in this manner show improved thermal resistance (13 °C/W compared with > 25 °C/W) and, most importantly, greatly improved stability of the thermal resistance. Figure I-7 shows the light output vs current for such a device from wafer 4-4-78 for heat-sink temperatures up to 71 °C (the highest temperature of operation yet achieved for a GaInAsP/InP laser). This device has been operating at the point indicated in Fig. I-7 (50 °C, 225 mA, 4 mW) for over 800 hr with no change in output power.

More-extreme tests of the stability of the thermal resistance in devices from high-threshold wafers were also carried out. One device was run CW at 50 °C with current densities between 8.1 and 8.6 kA/cm^2 for 107 hr; another was run at 40 °C with a current density of 9.1 kA/cm^2 for 709 hr (with no degradation) and then at 11.7 kA/cm^2 for 103 hr. Both devices eventually showed degradation which appeared to be due to increased internal leakage currents rather than increased thermal resistance. These studies are continuing.

J. N. Walpole
J. J. Hsieh
T. A. Lind

II. GaInAsP AND InP AVALANCHE PHOTODIODES

A. INVERTED MESA STRUCTURES

Moderate increases in avalanche gain and reductions in dark current have been achieved in GaInAsP/InP inverted mesa photodiode structures similar to those described in previous reports.[2] The $Ga_{0.80}In_{0.20}As_{0.50}P_{0.50}$ composition used gives a long-wavelength cutoff of about 1.3 μm. Value of gain as high as 18 with dark currents of 20 μA, at the same bias, have been measured. Breakdown voltages ranged from 30 to 150 V, depending on the carrier concentration in the GaInAsP layer (values of $N_D - N_A$ varied from 2×10^{15} cm^{-3} to 3×10^{16} cm^{-3}). No correlation was evident between achievable gain, dark current at high bias, and carrier concentration.

An acceptable explanation of the large dark current at biases sufficient to obtain gain is still lacking, even though the effect has also been observed by and continues to be a source of difficulty to workers at other laboratories.[3] The leakage current is quite low, $\lesssim 10^{-5}$ A/cm^2, at voltages up to about half the breakdown voltage, and then rises very rapidly with further increase in reverse bias. The increase is much more rapid than can be accounted for by the avalanche process, as measured by the photosignal gain.

The wide variation in the magnitude of the reverse current from diode-to-diode on the same wafer makes absolute comparisons difficult. However, it appears that at least in some wafers the leakage current scales with the area rather than the perimeter of the device, and is therefore a bulk as opposed to a surface effect. We are presently trying to develop a model to explain our results as well as examining the reverse characteristics of devices with different configurations, e.g., ion-implanted structures, for comparison.

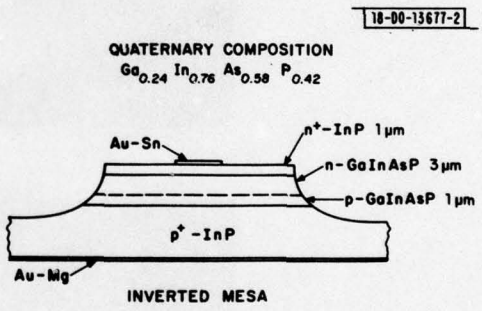

Fig. II-1. Schematic diagram of inverted mesa GaInAsP/InP avalanche photodiode structure.

Diodes fabricated from quaternary layers in the low 10^{15} cm^{-3} range have been operated at biases well above that required for the depletion region to "punch through" to the top n^+-InP layer (see Fig. II-1). These devices still show only moderate values of avalanche gain and substantial dark currents, but they have an extremely fast response to an optical signal. This is the result of the low capacitance associated with the wide depletion region and the fact that the carriers are generated directly in the high-field depletion region, thus eliminating diffusion effects. The response of one of these devices to an approximately 20-psec-wide (FWHM) pulse from a mode-locked $Nd_{0.5}La_{0.5}P_5O_{14}$ laser is shown in Fig. II-2. The device was mounted in a package originally designed for high-frequency operation of HgCdTe heterodyne-detector arrays,[4] as shown in Fig. II-3(a-b).

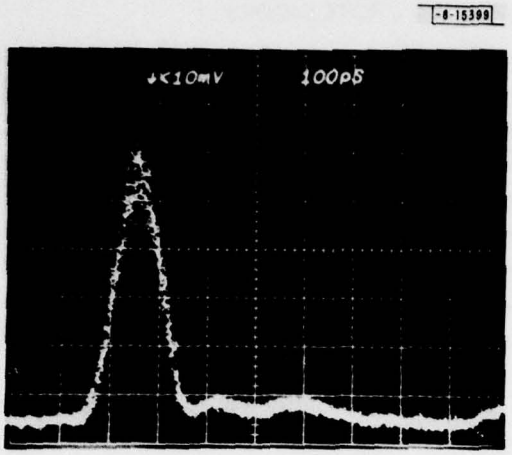

Fig. II-2. Response of GaInAsP/InP avalanche photodiode to 30-psec-wide pulse from mode-locked $Nd_{0.5}La_{0.5}P_5O_{14}$ laser. Bias voltage was 125 V, and detector was operated into 50-ohm load.

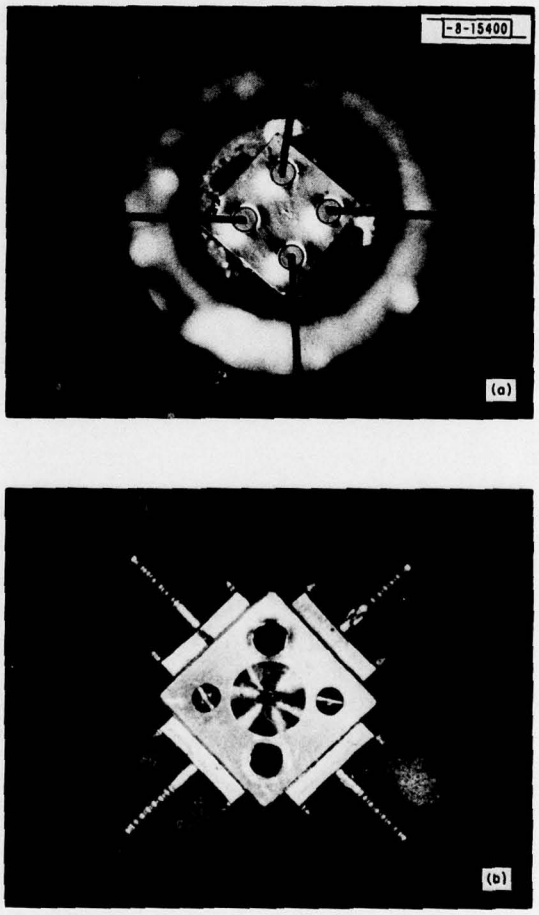

Fig. II-3. (a) Photograph of four GaInAsP/InP detectors mounted in (b) high-speed quad package.

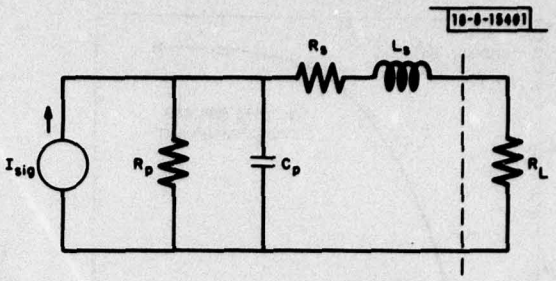

Fig. II-4. Equivalent circuit of packaged photodiode and load. See text for element values.

The 10- to 90-percent rise and fall times measured from the data in Fig. II-2 are 50 to 60 psec. The relevant parameters of a packaged device corresponding to the equivalent circuit of Fig. II-4 were measured on a network analyzer at 2 GHz. Values so obtained were C_p = 0.3 pF, R_s = 15 ohms, L_s = 0.5 nH, with the shunt resistance R_p being negligibly large. The calculated 10- to 90-percent response to a step input for this circuit operating into a 50-ohm load would be 30 psec. When combined with the 25-psec risetime of the oscilloscope, the approximately 15-psec risetime of the optical pulse, and the effect of the spread in transit time of carriers crossing the depletion layer (estimated to be ≈20 psec), the calculated response is in reasonable agreement with that measured. It should also be noted that the transparency of the InP top layer, together with the punched-through operation, results not only in very fast response but also in a high value of quantum efficiency (≈70 percent) which is limited primarily by the reflection loss at the InP-air interface.

The inverted mesa structure has also been employed successfully to fabricate promising avalanche diodes of InP. The configuration is similar to that of Fig. II-1, but consists simply of a 6-μm-thick layer of InP with $n \approx 9 \times 10^{15}$ cm^{-3}, grown epitaxially on a p^+-InP substrate. Measurements are only preliminary, but values of avalanche gain as high as 60 with dark currents at gain of 30 nA for a 6-mil-diam diode have been obtained. Further studies, including attempts to use these devices for ionization coefficient measurements, are in progress.

C. E. Hurwitz
C. A. Armiento
R. L. Payer

B. BERYLLIUM ION IMPLANTATION IN InP AND GaInAsP

Ion implantation is expected to play a significant role in the fabrication of avalanche photodiode structures in both InP and GaInAsP. Some preliminary results on both n- and p-type ion-implanted layers in InP have already been reported.[5-8] In this section, we will present more-detailed information on Be ion-implanted InP and report for the first time ion-implantation results in GaInAsP. The studies in InP include the effects of implant and anneal temperatures on the electrical characteristics of the implanted layers, and the effects on junction depth of the concentration of implanted Be ions. We will also report results on the use of a multi-energy Be-implant schedule designed to create a uniform-concentration p-type layer in both InP and GaInAsP. The latter results are applicable to the fabrication of high-quality p-n junctions, which are described in the following section.

The InP samples used in these experiments were cut from bulk single crystals. High-resistivity (111) Fe-doped samples were used for initial experiments, and (100) n-type samples

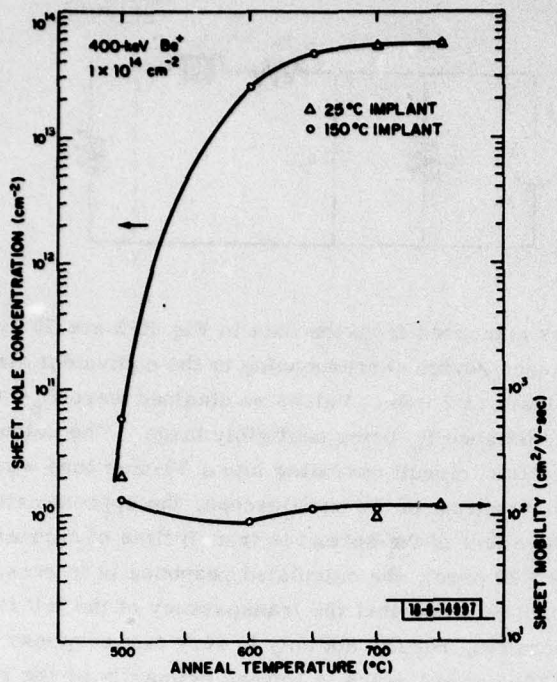

Fig. II-5. Sheet hole concentration and mobility vs anneal temperature for InP implanted with 1×10^{14} cm^{-2} 400-keV Be ions.

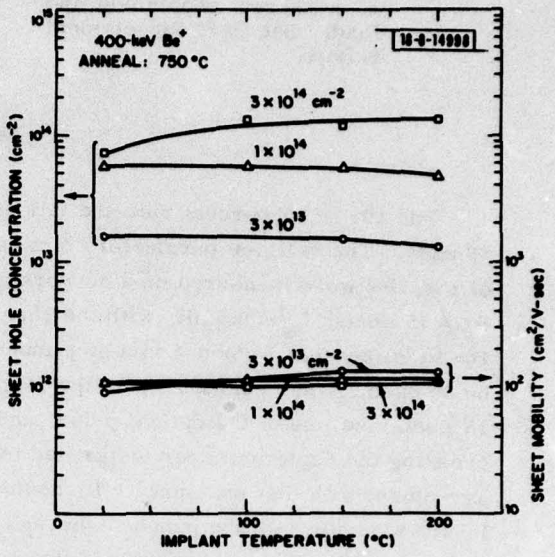

Fig. II-6. Sheet hole concentration and mobility vs implant temperature for InP implanted with 400-keV Be ions.

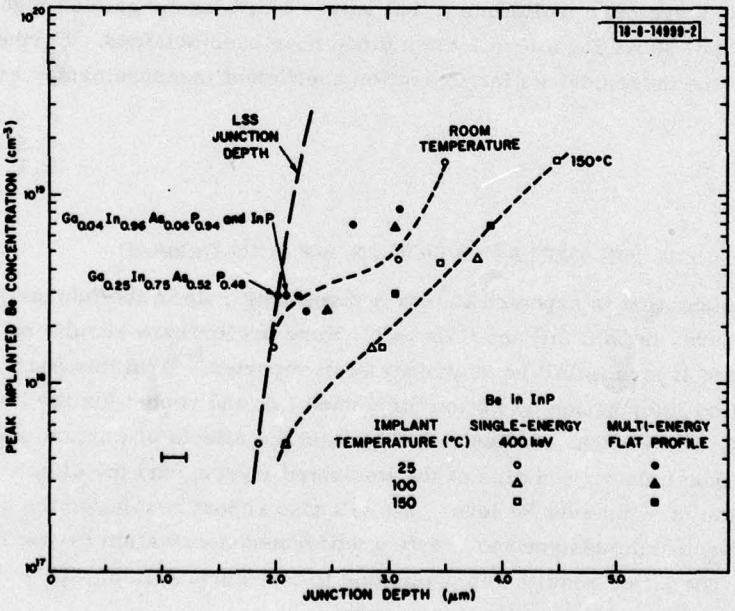

Fig. II-7. Junction depth vs maximum implanted Be concentration for 400-keV single- and multi-energy Be implants in InP and GaInAsP.

[$n \approx 2 \times 10^{16}$ cm^{-3}] were used for p-n junction measurements. After cutting and polishing, the InP samples were etched[9] in a 1:1:5:1 mixture of $HAc:HClO_4:HNO_3:HCl$. The GaInAsP samples used were n-type [$n \approx (0.5 \text{ to } 1) \times 10^{16}$ cm^{-3}] epitaxial layers grown by liquid-phase epitaxy on n^+-InP substrates.[10]

Beryllium was implanted into the etched surfaces of the InP samples and into the as-grown surfaces on the GaInAsP samples. Following implantation, two slightly different methods of encapsulation and anneal, which gave identical results on both implanted and control samples, were employed. Both methods rely on a pyrolytic phosphosilicate glass (PSG) encapsulation, nominally 7.84-wt% P, deposited at 250°C. Details of these methods and post-anneal sample processing can be found in Ref. 11.

For the first set of experiments, 400-keV Be^+ ions were implanted into Fe-doped substrates at temperatures ranging from room temperature to 200°C. The anneal temperatures used following implantation ranged from 500° to 750°C. Figure II-5 shows the sheet hole concentration and mobility vs anneal temperature for samples implanted at 150°C with 1×10^{14} cm^{-2} 400-keV Be ions. Data for several samples implanted at room temperature are also shown, and are in substantial agreement with 150°C data. As shown, there is a significant increase in the Be activation between 500° and 600°C. Between 600° and 700°C, the sheet hole concentration increases from 2.6×10^{13} to 5.3×10^{13} cm^{-2}. Following a 750°C anneal, the sheet concentration in samples implanted at 150°C was 5.6×10^{13} cm^{-2}, while in samples implanted at room temperature it was slightly higher at 5.9×10^{13} cm^{-2}.

Figure II-6 shows the sheet hole concentration and mobility vs implant temperature for samples implanted with several different doses of 400-keV Be ions and annealed at 750°C. The samples implanted with 3×10^{13} and 1×10^{14} cm^{-2} showed only a slight reduction in concentration with implant temperature. With a 3×10^{14} cm^{-2} implant, however, the sheet concentration in samples implanted at room temperature was about a factor-of-two lower than in samples implanted at $\geq$100°C.

To determine if these differences could be due to a Be-concentration dependent diffusion effect, as has been observed in GaAs (see Refs. 12 through 15), the junction depths in a series of n-type InP [$n \approx 2 \times 10^{16}$ cm^{-3}] samples implanted with both a single-energy (400-keV) and a multi-energy Be-implant schedule were determined. The multi-energy schedule was used since, in the actual fabrication of p-n junction diodes, some type of multiple implant would most likely be used to avoid the possibility of a buried p-type layer. The multi-energy schedule[16,17] used was designed to give a fairly uniform as-implanted Be concentration and was based on N at 400 keV, 12/18 N at 200 keV, 7/18 N at 100 keV, and 4/18 N at 50 keV, where N is the dose at 400 keV. For $N = 1.8 \times 10^{14}$ cm^{-2}, the uniform as-implanted Be concentration is about 3×10^{18} cm^{-3}. Following anneal and PSG removal, the samples were coated with $\approx$1000 Å of SiO_2 and then cleaved and preferentially etched in a KOH, $K_3Fe(CN)_6$ solution to reveal the position of the p-n junction.[18] The SiO_2-InP interface was used as the surface reference. The error in junction determination is estimated to be about 0.2 μm.

Figure II-7 shows the junction depth vs maximum implanted Be concentration (N_p) in InP samples implanted with either a single- or a multi-energy implant schedule and annealed at 750°C. The maximum implanted Be concentration was calculated from the implanted dose using LSS range theory.[16,17] Also shown is the junction depth in several GaInAsP samples implanted with a multi-energy implant schedule and annealed at 700°C. Note that one of the InP data points falls right on top of a GaInAsP data point. The heavy dashed line represents the junction depth

predicted from LSS theory in $n \approx 2 \times 10^{16}$ cm^{-3} InP. The predicted junction depths for the quaternary samples are very close to this line (within 0.05 μm). The light dashed lines are drawn through the single-energy room-temperature and 150°C implant results. Except for possibly the lowest dose, 3×10^{13} cm^{-2} ($N_p = 4.7 \times 10^{17}$ cm^{-3}), the junction depths in samples implanted at 100° and 150°C are significantly deeper than in similar samples implanted at room temperature. For the samples implanted at room temperature with a single-energy implant dose $\leq 1 \times 10^{14}$ cm^{-2} ($N_p \approx 1.6 \times 10^{18}$ cm^{-3}), the measured junction depths were identical to those predicted by LSS range theory, indicating insignificant indiffusion of the implanted Be. Samples implanted at room temperature with a multi-energy schedule, which resulted in an as-implanted concentration of 3×10^{18} cm^{-3}, exhibited junction depths which were within experimental error of that predicted by LSS theory. GaInAsP samples implanted to this level also showed insignificant Be indiffusion; however, samples implanted to higher Be concentration showed increased junction depth. For some reason which is not yet fully understood, the junction depth in samples implanted with a multi-energy Be implant were generally shallower than the junction depths in samples implanted with a single 400-keV implant. From the data, it appears that the maximum implanted Be concentration for a flat profile without significant indiffusion is about 3×10^{18} cm^{-3}. This result is qualitatively similar to results obtained on GaAs (see Refs. 12 through 15) and is in fairly good agreement with recently obtained SIMS measurements.[8]

TABLE II-1

MULTI-ENERGY BERYLLIUM IMPLANTS

(FLAT PROFILE $\approx 3 \times 10^{18}$ Be cm^{-3}) IN InP AND GaInAsP*

Material	Implant Temperature (°C)	Anneal Temperature (°C)	N_s (cm^{-2})	μ_s (cm^2/V-sec)
InP	25	700	1.3×10^{14}	62
InP	25	750	2.2×10^{14}	66
InP	150	750	1.8×10^{14}	87
$Ga_{0.24}In_{0.76}As_{0.52}P_{0.48}$	25	700	1.2×10^{14}	82
$Ga_{0.25}In_{0.75}As_{0.52}P_{0.48}$	25	700	1.5×10^{14}	81

*All samples implanted with 1.8×10^{14} cm^{-2} at 400 keV, 1.2×10^{14} cm^{-2} at 200 keV, 7.0×10^{13} cm^{-2} at 100 keV, and 4.0×10^{13} cm^{-2} at 50 keV.

Table II-1 summarizes the sheet carrier concentration and mobilities that have been obtained on n-type InP and GaInAsP samples implanted with the multi-energy Be schedule shown. This schedule should result in an as-implanted Be concentration of $\approx 3 \times 10^{18}$ cm^{-3}. For InP, the highest sheet concentration was obtained on samples implanted at room temperature and annealed at 750°C. As noted above, these samples showed insignificant indiffusion compared with samples

implanted at 150°C which had a lower sheet concentration. These results may indicate that outdiffusion to the surface also takes place when indiffusion is observed, as has been shown to take place in GaAs (see Ref. 14). Stripping measurements on a sample implanted at room temperature and annealed at 750°C indicate that the hole concentration is fairly uniform in the flat portion of the implanted region, with $p \approx (1.5 \text{ to } 2.0) \times 10^{18}$ cm^{-3}. Although the sheet concentrations obtained in quaternary samples which are annealed at 700°C are not as high as the best observed in InP, they are comparable to those obtained in the InP samples annealed at 700°C.

J. P. Donnelly G. A. Ferrante
C. A. Armiento S. H. Groves

C. BERYLLIUM-IMPLANTED STRUCTURES

In this section, we report results of p-n junction diodes formed by implantation of Be in n-type InP and GaInAsP. Mesa and planar InP diodes, which exhibit low leakage currents and abrupt breakdowns, have been fabricated. In addition, GaInAsP ($E_g \approx 1.0$ eV) mesa diodes have been made which exhibit uniform breakdown over the area of the device.

The InP and GaInAsP samples were selected and prepared as described in the preceding section where details of the implantation and anneal procedures are also found. Mesa diodes were fabricated by implanting the entire surface of the sample and subsequently etching mesas using a 1-percent bromine-methanol solution. Planar diodes were fabricated by implanting through holes opened in a 5-μm-thick layer of photoresist and a 2000-Å layer of pyrolytic SiO_2. In both structures, ohmic contacts to the p-type Be-implanted layers were made using evaporated and microalloyed Au-Mg. Contacts to the back of the n-type substrates were made using plated and microalloyed Au-Sn.

Initial diodes were fabricated using the following multi-energy Be-implant schedule: 1.8×10^{14} cm^{-2} at 400 keV, 1.2×10^{14} cm^{-2} at 200 keV, 7×10^{13} cm^{-2} at 100 keV, and 4×10^{13} cm^{-2} at 50 keV. According to LSS range theory,[16,17] this implant schedule should yield a fairly uniform as-implanted Be concentration of 3×10^{18} cm^{-3} and a junction depth of 2 μm. Measurement of the hole concentration in the implanted region and the junction depth have shown that this implant schedule results in insignificant indiffusion of the implanted Be (see Sec. B above).

Figures II-8(a) and (b) show the I-V characteristics of a 10-mil-diam mesa and a 15-mil-diam planar InP diode, respectively, fabricated using the above implant schedule. Leakage current in both diodes is in the subnanoampere range for reverse biases out to more than 10 V. Near breakdown, the etched mesa diodes exhibited significantly more leakage current than the planar diodes. A possible explanation is that the planar diodes had a pyrolytic SiO_2 layer over the exposed junction, which may have provided some surface passivation.

Similar mesa diodes fabricated in a 6-μm-thick layer of $Ga_{0.25}In_{0.75}As_{0.52}P_{0.48}$ ($n \approx 8 \times 10^{15}$ cm^{-3}) exhibited breakdown voltages as high as 92 V. Figure II-9 shows the effective concentration vs depletion width of such a $Ga_{0.25}In_{0.75}As_{0.52}P_{0.48}$ diode obtained from capacitance-voltage measurements. Using the abrupt depletion model, the effective concentration (N_{eff}) is equal to $N_A N_D/(N_A + N_D)$, where N_A and N_D are the net ionized acceptor and donor concentrations, respectively, at the edge of the depletion region. In the situation where $N_A \gg N_D$, N_{eff} vs depletion width is essentially a plot of net donor concentration as a function of distance. Figure II-9 indicates that the p-n junction is fairly abrupt. Although an exact fit has not been obtained, the slight grading that is observed is about what is expected from the as-implanted Be profile (which to first order falls off with a Gaussian shape).

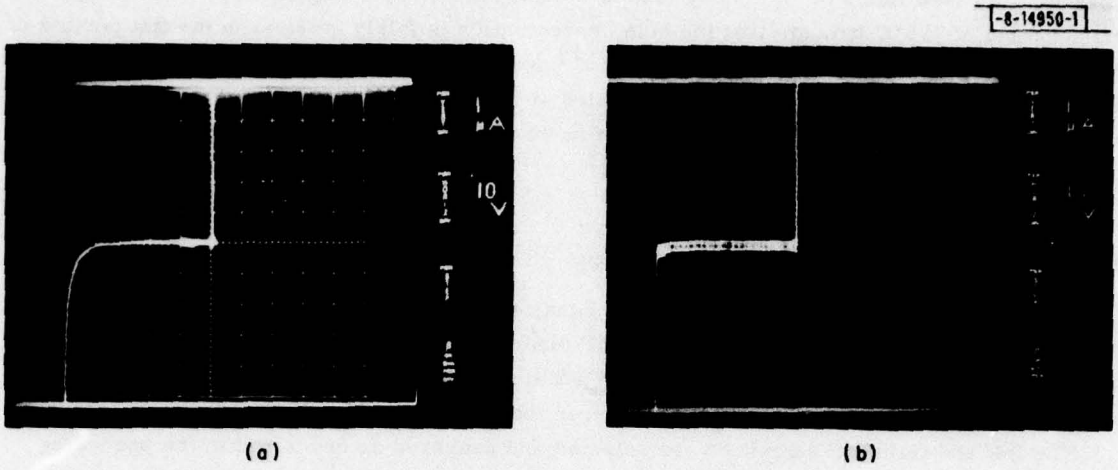

Fig. II-8. Current-voltage characteristics of Be-implanted InP diodes: (a) 10-mil-diam mesa diode; (b) 15-mil-diam planar diode.

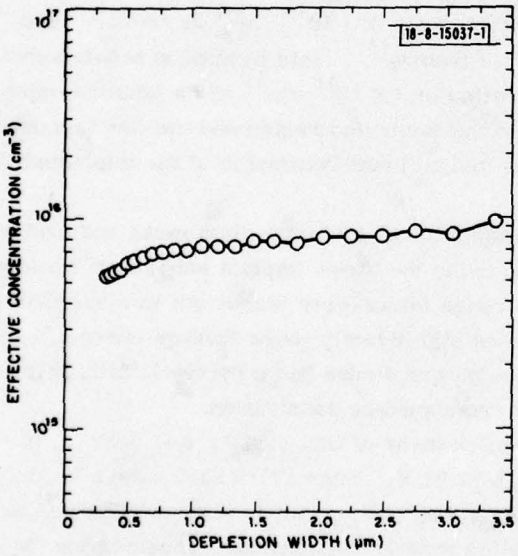

Fig. II-9. Effective concentration as a function of depletion width for a $Ga_{0.25}In_{0.75}As_{0.52}P_{0.48}$ mesa diode.

To determine if breakdown in the etched mesa InP and $Ga_{0.25}In_{0.75}As_{0.52}P_{0.48}$ diodes was due to uniform avalanche breakdown, scanned photoresponse measurements were performed using the 6328-Å line of a He-Ne laser. Although some of these diodes exhibited uniform photocurrent gains of up to three, many diodes showed edge breakdown and/or an enhanced edge response. As might be expected, inspection of the mesas indicated that the slope of the mesa at the junction generally determined whether or not a diode showed these edge effects.

To eliminate these edge effects so that the intrinsic uniformity of the Be-implanted junctions could be determined, diodes with shallower junctions were made in a thin GaInAsP layer which was "punched-through" or fully depleted before breakdown. The shallow junctions permit more-reproducible etching of mesas with near-vertical walls at the junction, which in turn minimize edge response and field crowding.[19] Punch-through operation further minimizes the effect of any residual field crowding.

The $Ga_{0.25}In_{0.75}As_{0.52}P_{0.48}$ layer used for these diodes was 4 μm thick and was implanted with Be doses of 6×10^{13} cm^{-2} at 70 keV and 5×10^{13} cm^{-2} at 50 keV. According to LSS range statistics, this implant schedule should yield a junction depth of 0.6 μm. Cleaved, stained mesas, however, indicate that some diffusion of Be has occurred, resulting in a junction depth of 1.2 to 1.5 μm.

Figure II-10 shows the effective concentration vs depletion width obtained from capacitance-voltage measurements on a 10-mil-diam etched mesa diode. Even though there was apparently some Be diffusion, these measurements indicate that the junction is still abrupt. The sudden increase in concentration at 2.5 μm indicates that the depletion region has reached through to the n^+-InP substrate. This punch-through occurs at 45 V, while breakdown occurs at 72 V.

Figures II-11(a) and (b) show the scanned photoresponse of one of these devices at a reverse bias of 69 V, taken using the 1.15-μm line of a He-Ne laser. Similar results were obtained using 0.6328-μm laser illumination. Figure II-11(a) shows the photoresponse superimposed on the raster scan pattern, while II-11(b) shows the horizontal scans superimposed on each other so that fluctuations in photoresponse are more easily detectable.

These scans indicate a uniform photoresponse gain of two (compared with the response at 50 V) over the entire area of the device, without any indication of edge response or edge breakdown. The depression in the photoresponse in the center of the device is due to the Au-Mg contact and the lead wire. These measurements indicate that junctions exhibiting uniform avalanche breakdown can be fabricated by Be-ion implantation.

C. A. Armiento
J. P. Donnelly
S. H. Groves

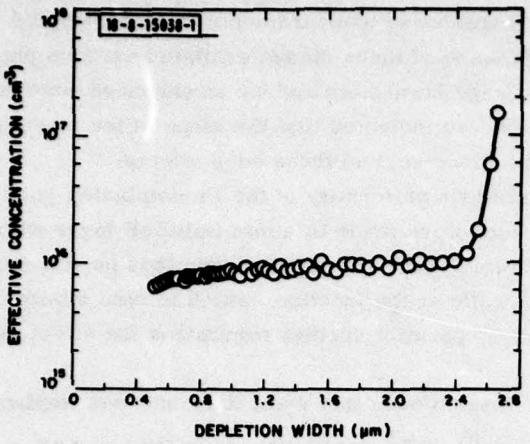

Fig. II-10. Effective concentration as a function of depletion width for a $Ga_{0.25}In_{0.75}As_{0.52}P_{0.48}$ punch-through mesa diode.

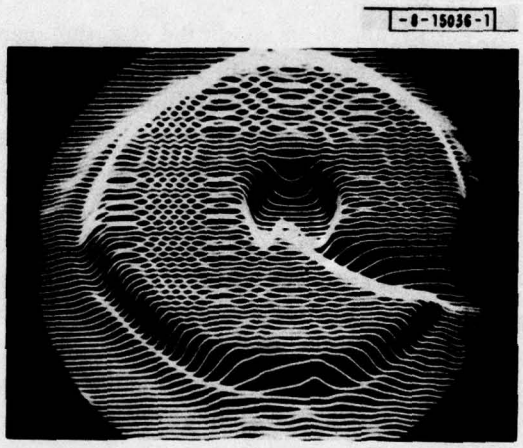

(a)

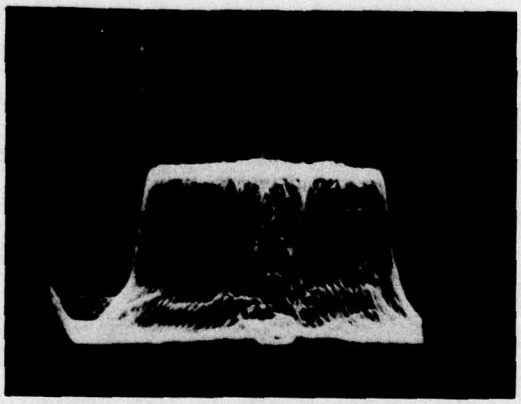

(b)

Fig. II-11. Photoresponse scans at 1.15 μm of a $Ga_{0.25}In_{0.75}As_{0.52}P_{0.48}$ punch-through mesa diode: (a) three-dimensional display; (b) two-dimensional display.

III. LPE GROWTH AND MATERIAL STUDIES OF InP AND GaInAsP

A. LPE GROWTH OF HIGH-PURITY InP AND GaInAsP LAYERS

High-quality, low-carrier-concentration material is essential for the successful fabrication of both avalanche and PIN photodiodes of InP and GaInAsP, as well as for the necessary and related studies of the electronic properties of three materials. In previous reports,[20] we discussed the role of silicon as the dominant donor impurity in LPE films of InP and GaInAsP and described some initial attempts to reduce the net impurity concentrations to low levels. Further work has resulted in the development of two simple and reproducible LPE growth techniques which have been used to grow both InP and GaInAsP layers with $N_D - N_A$ at the low 10^{15} cm^{-3} level. In this section we will describe the techniques in detail and discuss our current state-of-the-art results.

Our growth system is conventional in that it uses a horizontal, fused silica growth tube with a graphite slider, and the atmosphere is flowing H_2. Attention has been paid to the vacuum integrity of the joints – those on the upstream side of the growth tube are capable of operating under a vacuum of 10^{-8} Torr or lower, and those on the downstream side are capable of operating under a vacuum of 10^{-6} Torr or better. The system is operated in a mode where it is first evacuated with cooled molecular sieve pumps to 20 to 30 mTorr, checked for leaks by the rate of pressure rise, and then backfilled with H_2 from a Pd-alloy, diffusion-type purifier. Results presented here apply to a relatively clean growth tube, free from any noticeable buildup of phosphorous deposit.

As reported previously,[20] first attempts to grow undoped InP with this system were done with an extended prebake of the In at 900°C following suggestions in the literature. The InP grown at 600° to 700°C following this prebaking had high impurity concentrations, with $N_D - N_A \simeq 5 \times 10^{19}$ cm^{-3}. A mass spectrographic analysis showed that the prebake procedure had contaminated the In with Si in excess of 100 ppm which, with the large distribution coefficient reported[21] for Si ($k_{Si} \simeq 30$), was sufficient to account for the large value of $N_D - N_A$. Other evidence suggesting that Si is the dominant donor impurity has come from: (1) a correlation at moderate levels of purity, $1 \times 10^{16} < N_D - N_A < 1 \times 10^{17}$ cm^{-3}, between the Si content of the source In, as measured by mass spectroscopy, and values of $N_D - N_A$ (although, from the theory outlined below, these growth solutions cannot have fully equilibrated with the growth tube atmosphere); and (2) success at reducing $N_D - N_A$ below 1×10^{16} cm^{-3} by controlling the H_2O pressure, p_{H_2O}, in the growth tube atmosphere, as discussed below. Our conclusion about the importance of Si contamination for LPE growth of InP is in agreement with that of others.[22]

A general formulation of the problem of Si contamination of Ga solutions has been presented by Weiner.[23] One contamination mechanism, of several considered in that paper, undoubtedly applies to our situation of molten In in a graphite slider, under an atmosphere of H_2 in a fused silica growth tube:

$$SiO_2(s) + H_2(g) \rightleftharpoons SiO(g) + H_2O(g) \qquad [III\text{-}1(a)]$$

$$SiO(g) + 2In(l) \rightleftharpoons In_2O(g) + Si(l) \qquad [III\text{-}1(b)]$$

where s, l, and g indicate the solid, liquid, and gaseous phases, respectively. This mechanism, which transfers Si from the growth tube to the In solution via SiO, proceeds slowly because of the low pressures of the SiO generated, and times of order of 1000 hr are needed to

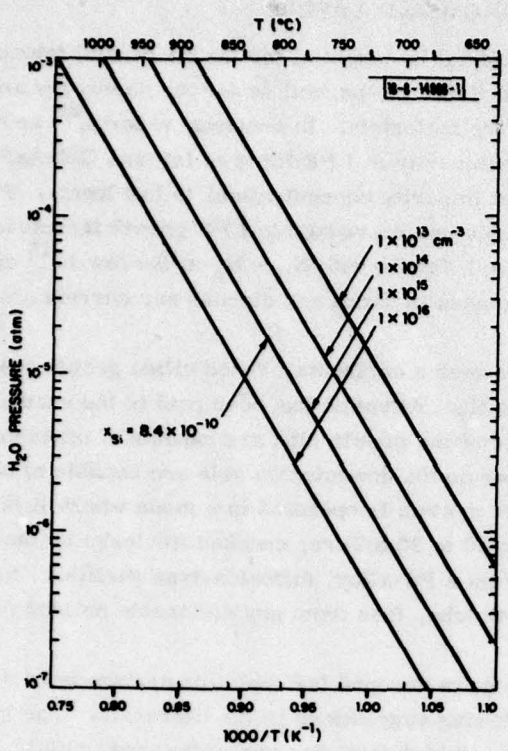

Fig. III-1. Calculated lines of constant x_{Si} labeled by donor concentration in LPE InP if $k_{Si} = 30$.

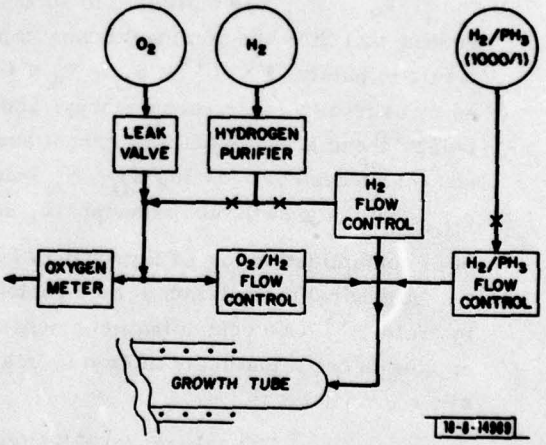

Fig. III-2. Schematic diagram of apparatus used for H_2O-addition and PH_3-source techniques.

reach equilibrium. This contamination process undoubtedly occurred in our experiments with the extended prebake at high temperatures.

A second process of direct contamination can occur if SiO_2 is in contact with the molten In:

$$SiO_2(s) + 4In(l) \rightleftharpoons 2In_2O(g) + Si(l) \quad . \tag{III-2}$$

The rate of this reaction is limited in the theory by the flow in In_2O vapor from the growth tube. In reality, the slower process of diffusion within the solution probably sets the rate. Times ranging from a few to 100 hr, depending upon the amount of convection and other mixing, are expected for equilibrium.

Whether one or both of these mechanisms is in effect, an equilibrium atomic fraction of Si in the solution x_{Si} will be established, and x_{Si} will depend only on the temperature and the H_2O vapor pressure in the gas entering the growth tube (or before the reduction of the SiO_2). This is shown in Fig. III-1, which results from calculations using thermodynamic data appropriate to In solutions.[24-26] The lines represent constant values of x_{Si}, but, using $k_{Si} = 30$ and assuming this independent of temperature, the lines are labeled by the value of expected donor concentration in the InP.

The assumptions of k_{Si} independent of temperature and only a single-donor species give an oversimplified picture that cannot explain all aspects of undoped LPE growth of InP. However, there are several experimental observations that are in reasonable agreement with the calculated values shown in Fig. III-1. First, from the temperature at which In_2O_3 is observed to be reduced in our system, we estimate that $p_{H_2O} \simeq 1 \times 10^{-7}$ atm. With this we see that a bake at 900°C is, indeed, expected to contaminate the growth with $N_D > 1 \times 10^{19}$ cm^{-3} (extrapolating three orders of magnitude to the left in Fig. III-1). Also, for growth of InP at 700°C we consistently grow material with N_D at the low 10^{16} cm^{-3} level.

The very low value of x_{Si} (below 1 ppb) necessary for growth at the 1×10^{15} cm^{-3} purity level is shown in Fig. III-1. The best commercially available In probably has 10 to 100 times this concentration of Si. Consequently, it is not sufficient to prevent contamination. The proper p_{H_2O} must be provided to purify the In, i.e., to drive the reactions of Eqs. (III-1) and (III-2) to the left. The reactions of Eqs. [III-1(a)] and [III-1(b)], with a long time constant, remove Si from the growth solution via the downstream flow of SiO. The long prebaking experiments of Wrick et al.[22] probably worked by this mechanism. Short-term (overnight) baking experiments, described below, provide evidence that the direct conversion of Si to SiO_2, Eq. (III-2), is also important.

Figure III-2 is a schematic drawing of our apparatus used for the H_2O-addition technique and the PH_3-source technique. The apparatus for controlling p_{H_2O}/p_{H_2} is similar to that used for LPE GaAs growth experiments.[27] O_2 is added through a leak valve to a flow of H_2, giving $p_{O_2} = 1 \times 10^{-5}$ atm. Most of this gas passes through an oxygen meter, and the remainder is accurately mixed with H_2 by means of flow-control valves. Essentially all the O_2 is converted to H_2O at the 650° to 700°C temperatures within the growth tube.

In Table III-1, we show the results of this technique for growth of InP and a GaInAsP alloy. The growth solution for InP (with liquidus temperature ≃ 700°C) is constituted from In and InP, and for GaInAsP (with liquidus temperature ≃ 650°C), GaAs and InAs are also used. All baking has been done at 700°C. The first row in each section gives results typical of those for growth

TABLE III-1
P_{H_2O}-ADDITION TECHNIQUE

InP				
Time (hr)	P_{H_2O} (atm)	$N_D - N_A$ (cm^{-3})	μ_{77} (cm^2/V-sec)	N_D/N_A
3 to 17	Dry	1.5×10^{16}	15,000	2.5
17	5×10^{-7}	2.6×10^{15}	52,000	–
65	5×10^{-7}	2.3×10^{15}	61,000	6.0
48	1×10^{-6}	1.5×10^{15}	70,000	–
17	$>1 \times 10^{-6}$	2.3×10^{15}	32,000	2.0
$In_{0.8}Ga_{0.2}As_{0.5}P_{0.5}$				
3 to 17	Dry	9.0×10^{15}	10,000	–
65	5×10^{-7}	1.3×10^{15}	14,000	–
17	1×10^{-6}	4.3×10^{15}	12,000	–
17	2×10^{-6}	7.8×10^{15}	11,000	–

TABLE III-2
PH_3-SOURCE TECHNIQUE

InP			
Time (hr)	$N_D - N_A$ (cm^{-3})	μ_{77} (cm^2/V-sec)	N_D/N_A
Unbaked	2.2×10^{16}	11,000	–
17	5 to 2×10^{15}	30,000 to 49,000	2.5
$In_{0.8}Ga_{0.2}As_{0.5}P_{0.5}$			
Unbaked	2.0×10^{16}	9,000	–
17	5 to 2×10^{15}	12,000 to 14,000	<2

in the dry H_2 atmosphere. A bake overnight in this atmosphere does not significantly change these values. For InP growth, an overnight bake with p_{H_2O} in the 5 to 10×10^{-7}-atm range causes $N_D - N_A$ to decrease to the low 10^{15} cm^{-3} level and causes μ_{77} to increase considerably. Increasing the bake time causes a small improvement. Although the ratio of N_D to N_A, determined from the mobility in the 20- to 50-K temperature range, was not measured for two growths, the high values of μ_{77} are an indication that they are only lightly compensated. Increasing p_{H_2O} does not significantly decrease $N_D - N_A$, and the compensation is greater than for the cases with p_{H_2O} between 5 and 10×10^{-7} atm.

In the case of the GaInAsP alloy, there appears to be a counter-doping effect caused by the H_2O (or O_2). The greatest reduction in $N_D - N_A$ is achieved for the fractional ppm range of H_2O. The values of μ_{77} improve only slightly, indicating that the atmosphere change and bake do not have a large effect on the total impurity concentration.

For the experiments with the PH_3-source technique, P is added to the InP or GaInAsP growth solutions from tank gas containing 10^{-3} parts PH_3 to 1 part H_2 (Fig. III-2). Typically, this mixture alone flows through the growth tube for 1 to 3 hr to constitute the growth solution, and then the flow is changed to the purified H_2 with only enough of the tank gas mixture to keep the substrate from thermally etching.

Table III-2 shows results using this technique. For InP growth, the solution is constituted from In and P from PH_3; and for GaInAsP growth, the required amounts of GaAs and InAs are also present. The liquidus and bake temperatures are the same as discussed above. The unbaked results are from growths made immediately after constituting the growth solution. These results are very similar to those in Table III-1 for growth in the dry H_2 atmosphere. If the constituted growth solution is baked overnight before the growth is made, the $N_D - N_A$ values for InP and GaInAsP drop to the low-to-mid 10^{15} cm^{-3} level, and the values of μ_{77} are about the same as with the H_2O-addition technique.

The PH_3-source technique, with behavior similar to that discussed above, was first used for growth of InP (see Ref. 28) and later extended to growth of GaInAsP alloys.[29] Evidently, the initial motivation for these experiments was to use a purer source of P than the bulk InP available at that time. However, no reason was offered for the required bake before growth.

On the basis of the similarity of results of the two growth methods discussed above and the following arguments, we believe that the PH_3-source technique works by the unintentional addition of H_2O. In support of this, we note that high-purity gases from cylinders typically contain 1 to 10 ppm of H_2O. A trap that is cold enough to reduce this H_2O concentration will also trap the PH_3. In rebuttal to the argument that PH_3 is a purer source of P than bulk InP, we first note that the number of electrically active donors in our bulk InP, $N_D \simeq 3 \times 10^{15}$ cm^{-3}, is insufficient to account for the number of donors in the LPE growth. It might be argued that inactive impurities in the bulk InP are active in the LPE growth and, to explain the necessity of the bake before growth, the argument put forth that PH_3 is free of Si but it contains a volatile impurity whose concentration is reduced by baking. Sulfur from H_2S might be such an impurity, as was suspected for growth of GaP using PH_3 (see Ref. 30). To check this possibility, we have run mass spectrographic analyses on baked and unbaked growth solutions. We cannot measure a significant difference between the two. Furthermore, with the exception of Si, the measured concentrations of all impurities whose distribution coefficients are known, or can be estimated, are too low to account for the 2×10^{16} cm^{-3} impurity level found in the unbaked growth. (The

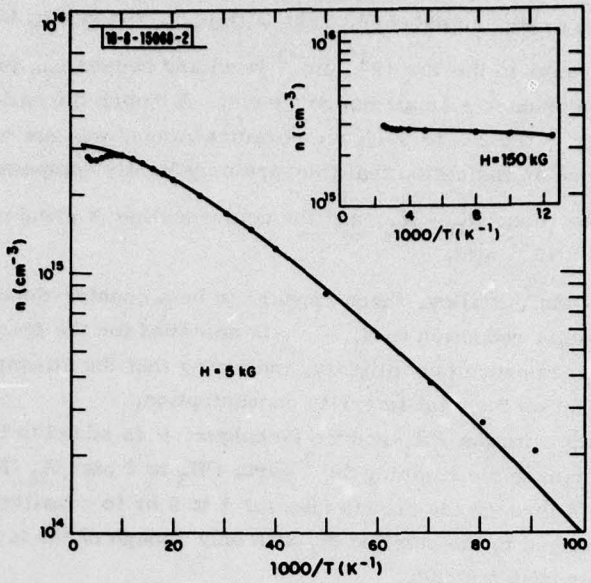

Fig. III-3. Effective electron carrier concentration vs 1000/T for InP. Solid curve is calculated using E_D = 3.7 meV. Inset shows high-magnetic-field data; curve is calculated using deep-level concentration of 5×10^{15} cm^{-3} and energy of 0.29 eV.

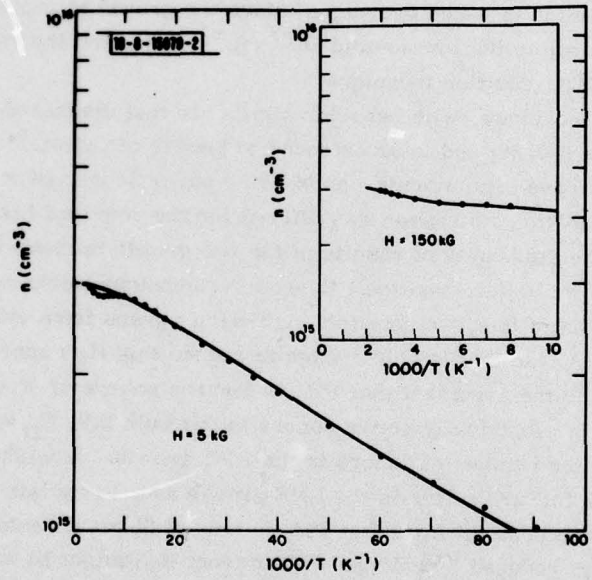

Fig. III-4. Effective electron carrier concentration vs 1000/T for $Ga_{0.2}In_{0.8}As_{0.5}P_{0.5}$. Solid curve is calculated using E_D = 0. Inset shows high-magnetic-field data; curve is calculated using deep-level concentration of 3×10^{14} cm^{-3} and energy of 0.12 eV.

concentration of Si, as determined by this analysis, is the same in baked and unbaked solutions, but this is expected because elemental Si and that from SiO_2 both contribute to the Si count.)

From this information, we believe that the PH_3-source growth works in the following manner: The large flow of tank gas increases p_{H_2O} in the growth tube. Over a time span of hours, part of the Si in the growth solution reacts to form SiO_2 because of the increased H_2O. A growth made immediately after loading the PH_3 will contain considerably more Si donors than a growth after a bake.

S. H. Groves
M. C. Plonko

B. TRANSPORT PROPERTIES AND IMPURITY LEVELS OF InP AND $Ga_{0.2}In_{0.8}As_{0.5}P_{0.5}$

Hall-coefficient and resistivity measurements as a function of temperature have been made on InP and $Ga_{0.2}In_{0.8}As_{0.5}P_{0.5}$ alloys grown by liquid-phase epitaxy (LPE). These materials were grown with one of the "in situ" purification procedures discussed in the previous section, and they have net, shallow impurity concentrations, $N_D - N_A$, in the low 10^{15} cm^{-3} range. Low-magnetic-field measurements were made at H = 5 kG with an automatic measurement apparatus[31] for temperatures between 10 and 300 K. The effective electron concentration n was determined from the measured Hall coefficient R by assuming that the Hall-coefficient scattering factor r is unity, i.e., n = r/Re = 1/Re, where e is the electronic charge. These data are shown by dots on the main plots in Fig. III-3 for InP and in Fig. III-4 for a $Ga_{0.2}In_{0.8}As_{0.5}P_{0.5}$ alloy.

A fit of the extrinsic carrier activation to the data of Figs. III-3 and III-4 has been accomplished by assuming a single-donor species and ignoring excited impurity states, as is appropriate to the range of purity considered here.[32] With these assumptions, the unknown parameters which determine the electron concentration are N_D, N_A, and E_D – the donor and acceptor concentrations and the donor activation energy, respectively. The quantity $N_D - N_A$ was estimated from the high-temperature n values in Figs. III-3 and III-4, and the individual values of N_D and N_A were then found from a mobility analysis,[32] based on the assumption that at some temperature the mobility is entirely limited by ionized impurity scattering. The conduction-band effective mass m_c^* and static dielectric constant ϵ_o used for this analysis are $m_c^* = 0.79\ m_o$ and $\epsilon_o = 12.4$ for InP, and $m_c^* = 0.061\ m_o$ and $\epsilon_o = 13.2$ for $Ga_{0.2}In_{0.8}As_{0.5}P_{0.5}$, where m_c^* for the alloy is taken from the magnetoabsorption results presented in Sec. D below, and ϵ_o for the alloy is estimated from an interpolation formula using the reported values of ϵ_o for GaAs, InP, InAs, and GaP. This procedure yielded the values: $N_D = 3.7 \times 10^{15}$ cm^{-3} and $N_A = 6.0 \times 10^{14}$ cm^{-3} for the InP sample using the fit to the mobility at $T \simeq 40$ K, and, for the alloy, $N_D = 6.0 \times 10^{15}$ cm^{-3} and $N_A = 3.0 \times 10^{15}$ cm^{-3} using the fit to the mobility at $T \simeq 20$ K. With these values of N_D and N_A in the charge neutrality equation, E_D was adjusted to give acceptable agreement between calculated and measured electron concentrations. The solid curves in the main portions of Figs. III-3 and III-4 are calculated for $E_D = 0.0037$ eV in the case of InP, and $E_D \simeq 0$ for $Ga_{0.2}In_{0.8}As_{0.5}P_{0.5}$. Boltzmann statistics are adequate for the InP case, but Fermi-Dirac statistics are necessary for the charge neutrality calculation in the case of the alloy. The deviation of the experimental points from the calculated curve at low temperatures, especially apparent in Fig. III-3, is due to the onset of competing conduction processes, such as impurity band conduction.

The behavior of the true electron concentration with temperature above 100 K for both the InP and GaInAsP alloy is obscured by the temperature dependence of the Hall-coefficient

scattering factor due to the increasing importance of polar mode phonon scattering above that temperature, an effect that has been studied in the case of high-purity GaAs (see Ref. 33). To separate the carrier activation from scattering effects, it is desirable to measure the Hall coefficient in the high-magnetic-field limit, $\mu H > 1 \times 10^8$, in which the scattering factor is unity. Measurements have been taken at the National Magnet Laboratory with H ≈ 150 kG, well into the high-field regime, for temperatures between 100 and 400 K, and the resulting data are plotted in the insets of Figs. III-3 and III-4. An effect that is difficult to see on the scale of these figures, but is present in all five samples measured, is the extra activation of electrons discernible at T > 250 K. To fit this, we have added a deep level of unknown energy and concentration to the charge balance equation. After some trial and error, we realized that deep levels giving a peak in the photoluminescence (see Sec. C below) for both InP and GaInAsP alloys were of the correct energies to produce the extra carrier activation if these levels were taken as lying closer to the conduction band than valence band. With the energy difference between near-band gap luminescence and the deep-level luminescence (0.29 eV for InP and 0.12 eV for GaInAsP), taken as the deep-level ionization energies, we can generate the curves shown in the insets of Figs. III-3 and III-4 with deep-level concentrations of 5×10^{15} cm^{-3} for InP and 3×10^{14} cm^{-3} for the GaInAsP alloy. The reduced number of these levels in the alloy compared with InP is in qualitative agreement with the intensities of the photoluminescence lines, shown in Sec. C.

An interesting possibility is that the deep level is due to oxygen. Several workers growing epitaxial InP have noticed that growth in an atmosphere with more O_2 or H_2O than usual causes an increase in the ratio of electron concentration at 300 K to that at 77 K. This effect may be caused by an increased number of these deep levels, although it is recognized that the concentration and ionization energy of the shallow donors as well as the compensation – factors that may vary with the O_2 or H_2O concentration in the growth tube atmosphere – also affect the quantity n_{300}/n_{77}.

S. H. Groves

C. PHOTOLUMINESCENCE OF InP AND $Ga_{0.2}In_{0.8}As_{0.5}P_{0.5}$ ALLOYS

A preliminary study has been made of photoluminescence from nominally undoped InP and $Ga_{0.2}In_{0.8}As_{0.5}P_{0.5}$ alloys grown by liquid-phase epitaxy (LPE). These measurements were made with the samples at 77 K and with an apparatus selected for ease of operation over a broad range of photon energies, 0.3 to 1.6 eV, at some sacrifice of resolution. A krypton laser provided photoexcitation of 0.5 W at 0.6741 μm wavelength. The luminescent radiation was passed through a prism monochromator and imaged on a thermoelectrically cooled PbS detector.

Figure III-5 shows the luminescence intensity vs photon energy for a sample of InP with electrical characteristics, $N_D - N_A = 2.8 \times 10^{15}$ cm^{-3} and $\mu_{77} = 3.7 \times 10^4$ cm^2/V-sec, where $N_D - N_A$ is the net impurity concentration and μ_{77} is the electron mobility at 77 K. The peak at ~1.4 eV involves transitions to shallow donors and acceptors and, under higher resolution, would separate into: (1) a sharp, high-intensity peak at 1.41 eV due to band-to-band and shallow-donor-to-valence-band transitions; (2) a weaker peak 35 to 40 meV below the first, due to conduction-band-to-shallow-acceptor transitions; and (3) possibly a transition 75 to 80 meV below the first, and very much weaker. These details can be seen in the spectra reported by workers at the Royal Radar Establishment for LPE-grown samples measured at 77 K (Ref. 34) and in measurements taken here at Lincoln Laboratory in an apparatus with higher resolution and with the samples near 4 K (Ref. 35). Very-high-resolution near-gap luminescence has also been reported for LPE InP samples at 1.8 K by Hess et al.[36]

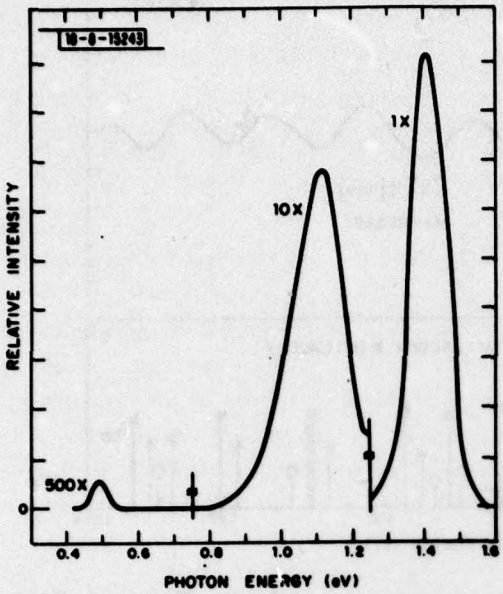

Fig. III-5. Photoluminescence spectrum for undoped InP grown by LPE.

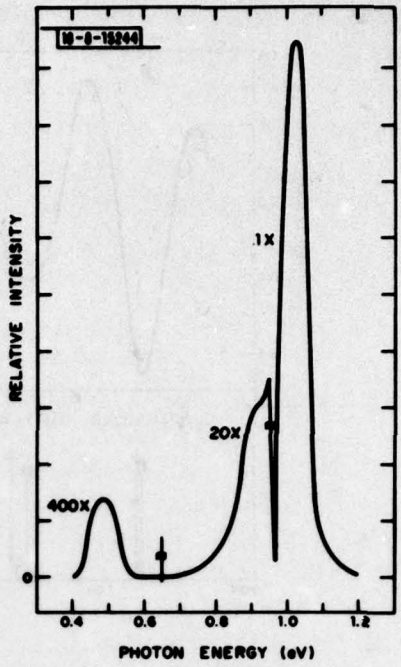

Fig. III-6. Photoluminescence spectrum for an undoped alloy of $Ga_{0.2}In_{0.8}As_{0.5}P_{0.5}$ grown by LPE.

The second peak in Fig. III-5, at 1.12 eV, is probably of the same origin as the broad peak at 1.17 eV in Ref. 34. This was seen in most, but not all, of the undoped LPE material investigated in that study and was seen in the bottom portion of their undoped, melt-grown InP crystals. The hypothesis was made in Ref. 34 that this line is the result of impurity/P-vacancy complexes. From our analysis of extrinsic carrier activation discussed in Sec. B above, we believe that this level is due to oxygen.

The lowest energy peak in Fig. III-5 occurs at 0.49 eV. Later runs with this apparatus were extended to 0.3 eV, and all samples showed, in addition, a similar type of transition at 0.35 eV. On the basis of an electron spin resonance (ESR) analysis,[37] the 0.35-eV line has been assigned to an intra-center transition between the $5T_2$ and 5E levels of the Fe^{2+} ($3d^6$) impurity. The origin of the 0.49-eV level is not known but may be radiation from a higher excited level of the Fe^{2+} manifold. Our undoped layers, 5 to 10 μm thick, were grown on the Fe-doped InP substrates. However, the possible role of the Fe in giving rise to the photoluminescence lines has not been determined.

Figure III-6 shows the luminescence spectrum for a $Ga_{0.2}In_{0.8}As_{0.5}P_{0.5}$ alloy with electrical characteristics $N_D - N_A = 5.8 \times 10^{15}$ cm^{-3} and $\mu_{77} = 1.2 \times 10^4$ cm^2/V-sec. The relative intensity scales in Figs. III-5 and III-6 are not necessarily the same, but probably are within a factor or 2 of each other. The main difference between the traces in Figs. III-5 and III-6, other than the energy shift due to the smaller bandgap of the alloy, is the reduced intensity in the second peak of Fig. III-6. Again, from the extrinsic activation analyses above, we attribute this

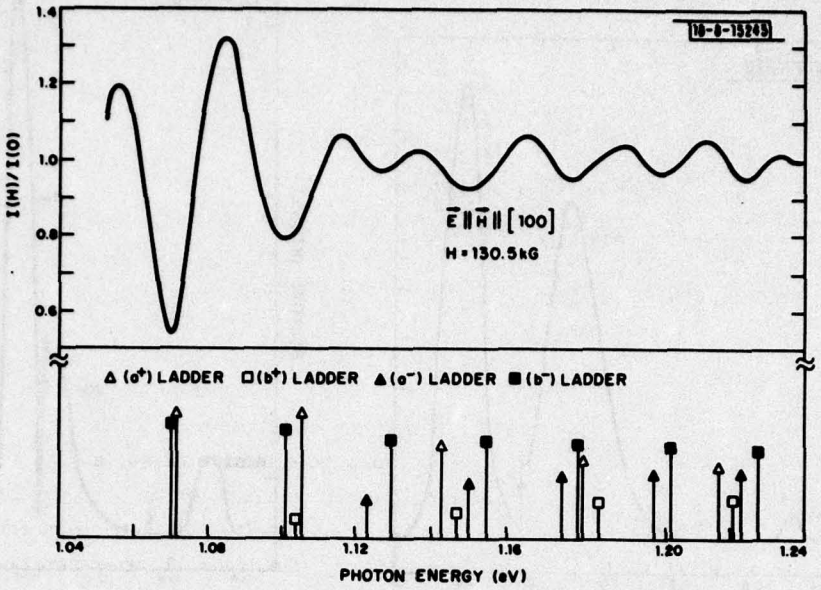

Fig. III-7. Voigt configuration magnetotransmission spectrum. Bars at bottom indicate theoretical energies, and their heights are proportional to square of matrix elements.

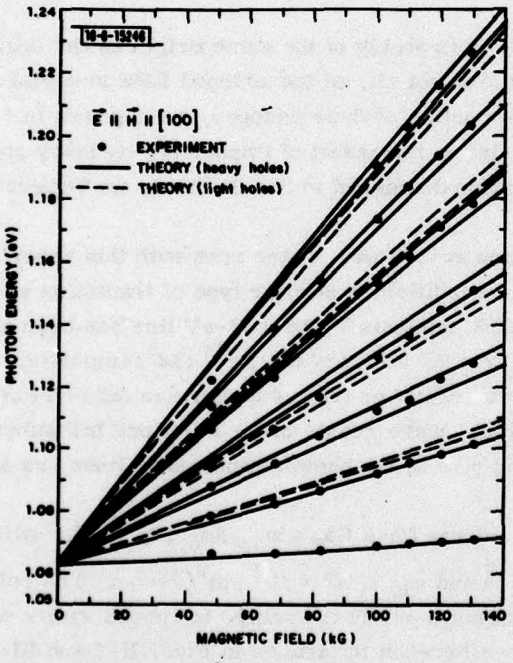

Fig. III-8. Transmission minima vs magnetic field. Theoretical curves include estimated excitation binding energy, which at H = 0 is 3 meV.

line to a level located 0.12 eV below the conduction band. The reduced concentration of this level in the alloy compared with that in InP is in qualitative agreement with the results of Sec. B above.

S. H. Groves
J. G. Mavroides
D. F. Kolesar

D. INTERBAND MAGNETOOPTICAL MEASUREMENTS ON GaInAsP ALLOYS

Oscillatory interband magnetotransmission in the 1.2-μm wavelength region has been measured on samples of $Ga_{0.23}In_{0.77}As_{0.52}P_{0.48}$ grown by liquid-phase epitaxy on InP substrates. Figure III-7 shows the oscillatory transmission made in the Voigt configuration, $\vec{E} \parallel \vec{H} \parallel [100]$, for H = 130.5 kG, and where $\vec{E}$ is the optical electrical field vector. The arrows show the energies and strengths of transitions predicted by the theory with band parameters determined from this study. Figure III-8 shows the spectrum generated by plotting energies of absorption minima vs H. The band parameters determined by the fit of theory to the experimental data are $E_g = 1.07$ eV, $m_c^* = 0.061\ m_o$, and $E_p = 17.6$ eV, where these parameters are, respectively, the direct energy gap at $T \approx 20$ K, the conduction-band effective mass, and the $\vec{k} \cdot \vec{p}$ interaction energy, proportional to the square of the momentum matrix element. We are presently extending the magnetooptical measurements both to other GaInAsP alloys lattice-matched to InP and to such techniques as electric-field-modulated magnetoreflection. A more-detailed report of this work has been accepted for publication.[38]

K. Alavi†
R. L. Aggarwal†
S. H. Groves

† Francis Bitter National Magnet Laboratory, M.I.T.

REFERENCES

1. Semiannual Technical Summary on Electrooptical Devices, Lincoln Laboratory, M.I.T. (31 March 1978), p. 1, DDC AD-A059062.
2. Ibid. (30 September 1977), p. 7, DDC AD-A054477/5; and p. 3 in Ref. 1.
3. See, for example, T. P. Lee, C. A. Burrus, and A. G. Dentai, in Technical Digest 1978 International Electron Devices Meeting, Washington, D. C. (IEEE, New York, 1978).
4. D. L. Spears, Infrared Phys. 17, 5 (1977), DDC AD-A046982/5.
5. J. P. Donnelly and C. E. Hurwitz, Appl. Phys. Lett. 31, 418 (1977), DDC AD-A050856/4.
6. D. Eirug Davies, J. P. Lorenzo, and T. G. Ryan, Solid-State Electron. 21, 981 (1978).
7. D. Eirug Davies, W. D. Putter, and J. P. Lorenzo, to appear in the December 1978 issue of the Journal of the Electrochemical Society.
8. W. J. Devlin, K. T. Ip, D. P. Leta, L. F. Eastman, G. H. Morrison, and J. Comas, presented at the 7th Intl. Symp. on GaAs and Related Compounds, St. Louis, Missouri, 24-27 September 1978.
9. R. Becker, Solid-State Electron. 16, 124 (1973).
10. S. H. Groves and M. C. Plonko, presented at the 7th Intl. Symp. on GaAs and Related Compounds, St. Louis, Missouri, 24-27 September 1978.
11. J. P. Donnelly and C. A. Armiento, to be published in Applied Physics Letters.
12. J. P. Donnelly, F. J. Leonberger, and C. O. Bozler, Appl. Phys. Lett. 28, 706 (1976), DDC AD-A028457/0.
13. J. Comas and L. Plew, J. Electron. Mater. 5, 209 (1976).
14. J. Comas, L. Plew, P. K. Chatterjee, W. V. McLevige, K. V. Vaidyanathan, and B. G. Streetman, in Ion Implantation in Semiconductors and Other Materials, F. Chernow, J. Borders, and D. Brice, Eds. (Plenum, New York, 1977), p. 141.
15. W. V. McLevige, M. T. Helix, K. V. Vaidyanathan, and B. G. Streetman, J. Appl. Phys. 48, 3342 (1977).
16. J. Lindhard, M. Scharff, and H. Schiott, K. Dan. Vidensk. Selsk., Mat.-Fys. Medd. 33, 1 (1963).
17. W. J. Johnson and J. F. Gibbons, Projected Range Statistics in Semiconductors (Stanford University Bookstore, Stanford, California, 1970).
18. R. L. Davies and F. E. Gentry, IEEE Trans. Electron Devices ED-11, 313 (1964).
19. M. G. Astles, F. G. H. Smith, and E. W. Williams, J. Electrochem. Soc. 119, 496 (1972).
20. Semiannual Technical Summary on Electrooptical Devices, Lincoln Laboratory, M.I.T. (31 March 1977), p. 11, DDC AD-A046483/4; and (31 March 1978), p. 9, DDC AD-A059062.
21. G. G. Baumann, K. W. Benz, and M. H. Pilkuhn, J. Electrochem. Soc. 123, 1232 (1976).
22. V. L. Wrick, K. T. Ip, and L. F. Eastman, J. Electron. Mater. 7, 253 (1978).
23. M. E. Weiner, J. Electrochem. Soc. 119, 496 (1972).
24. Janaf 1965, Thermochemical Tables (U.S. Dept. of Commerce).
25. A. Klinedinst and D. A. Stevenson, J. Chem. Thermodynam. 5, 21 (1973).
26. P. H. Keck and J. Broder, Phys. Rev. 90, 521 (1953).

27. H. G. B. Hicks and P. D. Greene, Gallium Arsenide and Related Compounds 1970, Inst. Phys. Conf. Ser. 9, 92 (1971).

28. M. G. Astles, F. G. H. Smith, and E. W. Williams, J. Electrochem. Soc. 120, 1750 (1973).

29. R. Sankaran, G. A. Antypas, R. L. Moon, J. S. Escher, and L. W. James, J. Vac. Sci. Technol. 13, 932 (1976).

30. C. M. Ringle, J. Electrochem. Soc. 118, 609 (1971).

31. Semiannual Technical Summary on Electrooptical Devices, Lincoln Laboratory, M.I.T. (31 March 1978), p. 11, DDC AD-A059062.

32. G. E. Stillman and C. M. Wolfe, Thin Solid Films 31, 69 (1976), DDC AD-A024175/2.

33. G. E. Stillman, C. M. Wolfe, and J. O. Dimmock, J. Phys. Chem. Solids 31, 1199 (1970), DDC AD-714321.

34. J. B. Mullin, A. Royle, B. W. Straughan, P. J. Tufton, and E. W. Williams, J. Cryst. Growth 13/14, 640 (1972).

35. A. R. Calawa, J. V. Gormley, and S. H. Groves, unpublished results.

36. K. Hess, N. Stath, and K. W. Benz, J. Electrochem. Soc. 121, 1208 (1974).

37. W. H. Koschel, U. Kaufmann, and S. G. Bishop, Solid State Commun. 21, 1069 (1977).

38. K. Alavi, R. L. Aggarwal, and S. H. Groves, to be published in the Journal of Magnetism and Magnetic Materials.

UNCLASSIFIED

SECURITY CLASSIFICATION OF THIS PAGE (When Data Entered)

REPORT DOCUMENTATION PAGE		READ INSTRUCTIONS BEFORE COMPLETING FORM
1. REPORT NUMBER ESD-TR-78-394	2. GOVT ACCESSION NO.	3. RECIPIENT'S CATALOG NUMBER
4. TITLE (and Subtitle) Electrooptical Devices		5. TYPE OF REPORT & PERIOD COVERED Semiannual Technical Summary rept. 1 April – 30 September 1978
		6. PERFORMING ORG. REPORT NUMBER
7. AUTHOR(s) Charles E. Hurwitz		8. CONTRACT OR GRANT NUMBER(s) F19628-78-C-0002
9. PERFORMING ORGANIZATION NAME AND ADDRESS Lincoln Laboratory, M.I.T. P.O. Box 73 Lexington, MA 02173		10. PROGRAM ELEMENT, PROJECT, TASK AREA & WORK UNIT NUMBERS Program Element Nos. 62702F and 61102F Project No. 261104
11. CONTROLLING OFFICE NAME AND ADDRESS Rome Air Development Center Griffiss AFB, NY 13440		12. REPORT DATE 30 September 1978 13. NUMBER OF PAGES 38
14. MONITORING AGENCY NAME & ADDRESS (if different from Controlling Office) Electronic Systems Division Hanscom AFB Bedford, MA 01731		15. SECURITY CLASS. (of this report) Unclassified 15a. DECLASSIFICATION DOWNGRADING SCHEDULE

16. DISTRIBUTION STATEMENT (of this Report)

Approved for public release; distribution unlimited.

16) 2611

17) 04

17. DISTRIBUTION STATEMENT (of the abstract entered in Block 20, if different from Report)

18. SUPPLEMENTARY NOTES

None

19. KEY WORDS (Continue on reverse side if necessary and identify by block number)

electrooptical devices	proton bombardment	ion implantation
avalanche photodiodes	double-heterostructure	GaInAsP/InP lasers

20. ABSTRACT (Continue on reverse side if necessary and identify by block number)

This report covers work carried out with support of the Department of the Air Force during the period 1 April through 30 September 1978. A part of this support was provided by the Rome Air Development Center.

The current objectives of the electrooptical device program are: (1) to perform life tests on GaInAsP/InP double-heterostructure (DH) diode lasers operating in the 1.0- to 1.3-μm-wavelength region and analyze the degradation mechanisms, and (2) to fabricate and study avalanche photodiodes of similar composition GaInAsP operating in the same wavelength region.

2 on next page

DD FORM 1 JAN 73 1473 EDITION OF 1 NOV 65 IS OBSOLETE

UNCLASSIFIED

SECURITY CLASSIFICATION OF THIS PAGE (When Data Entered)

207 650

LB

20. ABSTRACT (Continued)

Threshold current densities in DH GaInAsP/InP stripe geometry lasers have been reduced to 2 to 3 kA/cm^2, which, together with new mounting procedures designed to reduce thermal resistance, have resulted in improved performance at elevated temperatures. Considerably lengthened lifetimes and meaningful accelerated aging studies at temperatures as high as 70°C should now be possible.

Values of gain as high as 18 with concurrent dark currents of 20 μA have been achieved in GaInAsP/InP inverted mesa photodiodes. Rise and fall times of less than 60 psec in detector pulse response have been measured.

Multi-energy Be implants in n-type InP and GaInAsP have yielded layers with uniform as-implanted Be concentrations of approximately 3×10^{18} cm^{-3}. Sheet carrier concentrations of 1 to 2×10^{14} cm^{-2} were obtained on samples implanted at room temperature and annealed at 750° and 700°C for InP and GaInAsP, respectively.

Improved p-n junction diodes have been formed by Be-implantation in n-type InP and GaInAsP. Sub-nanoampere leakage currents and abrupt voltage breakdowns were observed for both mesa and planar InP diodes. Scanning photoresponse measurements of the GaInAsP ($E_g \approx 1.0$ eV) mesa diodes showed uniform avalanche gains of 2 to 3 times.

Liquid-phase epitaxy is now being used to reproducibly grow InP and GaInAsP alloys with $N_D - N_A$ at the low 10^{15} cm^{-3} level. The 77 K electron mobilities for the InP are in the 40,000 to 60,000 cm^2/V-sec range, with N_D/N_A between 2.5 and 6. For $Ga_{0.2}In_{0.8}As_{0.5}P_{0.5}$, the 77 K mobilities are 12,000 to 14,000 cm^2/V-sec with $N_D/N_A \leq 2$.

Analysis of measurements of the high-magnetic-field Hall coefficient vs temperature yields values for the concentrations of deep donors in InP and GaInAsP specimens of 5×10^{15} cm^{-3} and 3×10^{14} cm^{-3}, respectively. The transport data were fit using deep-level donor activation energies of 0.29 and 0.12 eV for InP and GaInAsP, respectively. These energy values were inferred from the photoluminescence spectra.

In a study of photoluminescence of LPE-grown InP and GaInAsP, several spectral peaks were observed in a range 0.3 to 1.41 eV. It is hypothesized that one of the peaks in the photoluminescence spectra, with peak energies of 1.12 eV for InP and 0.9 eV for GaInAsP, is due to oxygen.

The oscillatory interband magnetotransmission has been measured on samples of LPE-grown $Ga_{0.23}In_{0.77}As_{0.52}P_{0.48}$ layers. The band parameters determined from the analysis of the data are $E_g = 1.07$ eV, $m_c^* = 0.061\ m_o$, and $E_p = 17.6$ eV, where these parameters are the direct energy gap at $T \approx 20$ K, the conduction-band effective mass, and the $\vec{k} \cdot \vec{p}$ interaction energy, respectively.